ACS central science

Research Article

Cite This: ACS Cent. Sci. 2018, 4, 1113−1125

Resolving the Core and the Surface of CdSe Quantum Dots and Nanoplatelets Using Dynamic Nuclear Polarization Enhanced PASS−PIETA NMR Spectroscopy

Laura Piveteau,[†,‡] Ta-Chung Ong,[†,#] Brennan J. Walder,[§] Dmitry N. Dirin,[†,‡] Daniele Moscheni,[∥] Barbara Schneider,[†] Janine Bär,[†] Loredana Protesescu,[†,‡,▽] Norberto Masciocchi,[∥] Antonietta Guagliardi,[∥,⊥] Lyndon Emsley,[§] Christophe Copéret,*[,†] and Maksym V. Kovalenko*[,†,‡]

[†]Department of Chemistry and Applied Biosciences, ETH Zürich, Vladimir Prelog Weg 1-5, CH-8093 Zürich, Switzerland

[‡]Empa-Swiss Federal Laboratories for Materials Science and Technology, Dübendorf, Überlandstrasse 129, CH-8600 Dübendorf, Switzerland

[§]Institut des Sciences et Ingénierie Chimiques, Ecole Polytechnique Fédérale de Lausanne (EPFL), 1015 Lausanne, Switzerland

[∥]Dipartimento di Scienza e Alta Tecnologia and To.Sca.Lab, Università dell'Insubria, via Valleggio 11, I-22100 Como, Italy

[⊥]Istituto di Crystallografia and To.Sca.Lab, Consiglio Nazionale delle Ricerche, via Valleggio 11, I-22100 Como, Italy

Supporting Information

ABSTRACT: Understanding the surface of semiconductor nanocrystals (NCs) prepared using colloidal methods is a long-standing goal of paramount importance for all their potential optoelectronic applications, which remains unsolved largely because of the lack of site-specific physical techniques. Here, we show that multidimensional ^{113}Cd dynamic nuclear polarization (DNP) enhanced NMR spectroscopy allows the resolution of signals originating from different atomic and magnetic surroundings in the NC cores and at the surfaces. This enables the determination of the structural perfection, and differentiation between the surface and core atoms in all major forms of size- and shape-engineered CdSe NCs: irregularly faceted quantum dots (QDs) and atomically flat nanoplatelets, including both dominant polymorphs (zinc-blende and wurtzite) and their epitaxial nanoheterostructures (CdSe/CdS core/shell quantum dots and CdSe/CdS core/crown nanoplatelets), as well as magic-sized CdSe clusters. Assignments of the NMR signals to specific crystal facets of oleate-terminated ZB structured CdSe NCs are proposed. Significantly, we discover far greater atomistic complexity of the surface structure and the species distribution in wurtzite as compared to zinc-blende CdSe QDs, despite an apparently identical optical quality of both QD polymorphs.

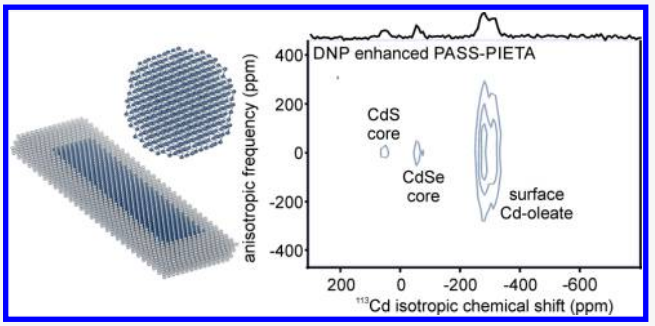

INTRODUCTION

Semiconductor nanocrystals (NCs) prepared via colloidal approaches are materials of interest to diverse scientific communities due to their unique photophysical and electronic properties[1,2] and emerging commercial applications such as in television displays (Samsung, Sony, and several other major companies). With at least one dimension smaller than their exciton Bohr radius, they also exhibit quantum-size effects in their optical and electronic properties; they thus often are called by their alternative names—quantum dots (QDs, sub-20 nm NCs, confined in three dimensions), quantum wells (or nanoplatelets, NPLs, which are atomically flat, sub-10 nm thick NCs), or quantum wires (nanowires, typically sub-20 nm thick). These small crystallites are inherently high-surface-area materials, whose surface is a key player in the material's physical and chemical behavior.[3−8] Effects from NC cores and surfaces are practically never independent of each other, be it synergistic or counteracting with respect to observable physical properties. For instance, radiative recombination of electron−hole pairs, generated in the NC core, is nearly always negatively influenced by the surface states, localized on the undercoordinated surface atoms, leading to diminishing of the photoluminescence quantum yield and/or emergence of trap-related photoluminescence bands. On a positive note, rationally engineered surface traps have enabled high photoconductivity in densely packed solids of NCs.[9−11] Characterizing and understanding surfaces of semiconductor NCs are therefore necessary to rationally control and tune their properties, eventually enabling numerous applications in electronics[12−15] and optoelectronics (light-emitting diodes, photodetectors, photovoltaics, lasers,

Received: March 31, 2018
Published: June 25, 2018

DOI: 10.1021/acscentsci.8b00196
ACS Cent. Sci. 2018, 4, 1113−1125

and many more),[1,6,9−11,16−26] photocatalysis,[27−29] photoelectrochemistry,[30] and life sciences (as luminescent labels).[3,31−34]

Colloidal semiconductor NCs typically comprise three regions: a crystalline core, a NC surface region, and molecular ligands, which are covalently attached to the NC surface. These ligands ensure chemical integrity of the NC and colloidal stability in apolar and polar solvents, and may serve as a platform for further functionalization. Because the complexity of these entities exceeds those of smaller, atomically defined molecules and extended solids, a typical characterization toolbox consists of a diversity of methods applied in a combined manner: in particular, transmission electron microscopy (TEM), X-ray scattering methods (in the small- and wide-angle region, pair-distribution-function analysis, etc.), photoelectron spectroscopies, X-ray absorption and fluorescence, thermal analysis (thermogravimetric analysis, differential scanning calorimetry, etc.), Fourier-transform infrared spectroscopy, nuclear magnetic resonance spectroscopy (NMR), and optical characterization by absorption and emission spectroscopies. Among these, NMR techniques continue to hold a prominent position with great potential for further development. Solid-state and solution NMR, widely used in chemistry and materials science, is capable of providing a full description in terms of atomic connectivity, oxidation state, geometry of local environment created by other atoms, as well as dynamics for a broad range of systems: organic/inorganic, crystalline/amorphous, surface, or the core. Unsurprisingly, NMR has been widely used over the last two decades for characterizing colloidal semiconductor NCs, foremost for characterizing semiconductor NC surface ligands.[35−54] When molecular capping ligands are observed, the information obtained by conventional solution NMR rapidly diminishes once the molecular tumbling is restricted, e.g., upon binding, from the free dissolved state to the surface. The greatest utility of solution NMR thus far has been in observing and quantifying the binding dynamics of organic ligands at the NC surfaces.[35−42] Solid-state NMR, on the contrary, can probe all magnetically active nuclei in a statistically averaged ensemble of semiconductor NCs.[43,45,46,48−51,55−58] For example, for various WZ-CdSe, ZB-CdSe, and InP QDs, assignments of the core and surface $^{111/113}$Cd, ^{77}Se, and ^{31}P species were proposed.[43,45,48,50,56] Berrettini et al. identified five different ^{77}Se species in WZ-CdSe QDs, one tetrahedrally coordinated within the core region and the others being rather surface species (vertex, edge, and on two different facets).[56] Furthermore, two possible ligand attachment modes were elucidated on the basis of their NMR spectra.[56]

However, NMR in general, and its applications to inorganic materials in particular, suffers from inherently poor sensitivity, especially for isotopes that are low in natural abundance or have a low gyromagnetic ratio. The sensitivity problem culminates on NC surfaces, wherein additional factors reducing the NMR signal intensities are various inhomogeneities and overall reduced number of atoms.

It was recently shown that solid-state NMR measurements, exploiting signal enhancements from dynamic nuclear polarization (DNP),[59−65] can be conducted directly on colloidal semiconductor NC solutions (InP, CdSe, CdTe, PbSe, PbTe QDs).[50,66] This approach transfers electron polarization from a stable radical, added to a NC solution, to the nuclei of interest. DNP NMR experiments are optimal at low temperatures (approximately 100 K) where electron and nuclear relaxation rates are reduced.[67,68] For the avoidance of NC aggregation in low-temperature experiments, NC colloids have been impregnated first into nanosized pores of mesoporous silica (meso-SiO_2).[50] This sample preparation method was a key for maximizing the signal enhancement, as it ensures that NCs and organic radicals remain homogeneously mixed throughout the experiment. Enhancement factors of 56 were obtained for ^{31}P nuclei of InP NCs at a magnetic field of 9.4 T.[50] For challenging cases such as CdSe NCs, DNP enhanced NMR was the only method for obtaining and resolving the $^{111/113}$Cd signal from the NC surface. With just 1−2 mg of NCs in a native colloidal state, DNP enhanced spectra can be acquired within minutes for simple one-dimensional (1D) NMR spectra and within hours for more complex experiments including two-dimensional (2D) NMR spectroscopy. Other formulations suited for DNP experiments on colloidal nanomaterials include incorporation into acrylamide gels[66] or impregnation with meso-SiO_2 for which nitroxide radicals were incorporated into the walls of the pores.[69]

In addition to the need for sensitivity enhancement, another major challenge is to extract useful information from the broad and overlapping signals: a problem inherent to all NCs. Because of the small size and the high surface area, the environmental anisotropy is large for every single spin in the NC. This results in significant inhomogeneous broadening. In ordered solids, this can be addressed by magic-angle spinning (MAS), where the broad pattern splits into a manifold of relatively sharp spinning sidebands flanking the centerband at integer multiples of the rotation rate. However, when distributions of isotropic resonances are present, the one-dimensional MAS NMR spectra will consist of interdigitated sideband manifolds, and spectral resolution will not be significantly improved. To retain the information from chemical shift anisotropy (CSA) while obtaining a high-resolution spectrum from the isotropic components, the principles of sideband separation, introduced by Dixon,[70] can be implemented in the form of 2D NMR experiments. The archetypical experiments of this class are the closely related 2D phase adjusted spinning sideband (2D PASS)[71] and magic-angle turning (MAT)[72−74] experiments. The MAT archetype, in particular, has been the subject of numerous extensions,[71,75−77] having been adapted even to broadband refocusing pulses[78] and indirect detection;[79] however, 2D PASS should be the preferred experiment when transverse coherence lifetimes are comparable to or shorter than the sample rotation period.[71]

In this work, we demonstrate how 2D PASS experiments, enhanced by phase-incremented echo-train acquisition (PIETA),[80] allow discerning isotropic chemical shifts of various ^{113}Cd species existing in well-defined Cd-chalcogenide NCs of various morphologies and evaluation of the anisotropy of these ^{113}Cd species. Our implementation is improved by the incorporation of surface-based hyperpolarization using DNP NMR:[59,60,63,67] a strategy which has already been adapted to MAT and PASS experiments.[81−83,66] We refer to the combined experiment as DNP enhanced PASS-PIETA, which affords 2D sideband correlation spectra at over 100-fold improvement in NMR sensitivity relative to the conventional 2D PASS. In particular, we use DNP enhanced PASS−PIETA to characterize the surface sites in CdSe-based nanostructures, a canonical family of semiconductor NCs. Diverse NC morphologies were probed, ranging from magic-sized clusters to sub-10 nm NCs and atomically smooth NPLs. In particular, sub-10 nm CdSe NCs, crystallized in both polymorphs (zinc-blende, ZB; and wurtzite, WZ), were characterized and compared to the core/

DOI: 10.1021/acscentsci.8b00196
ACS Cent. Sci. 2018, 4, 1113−1125

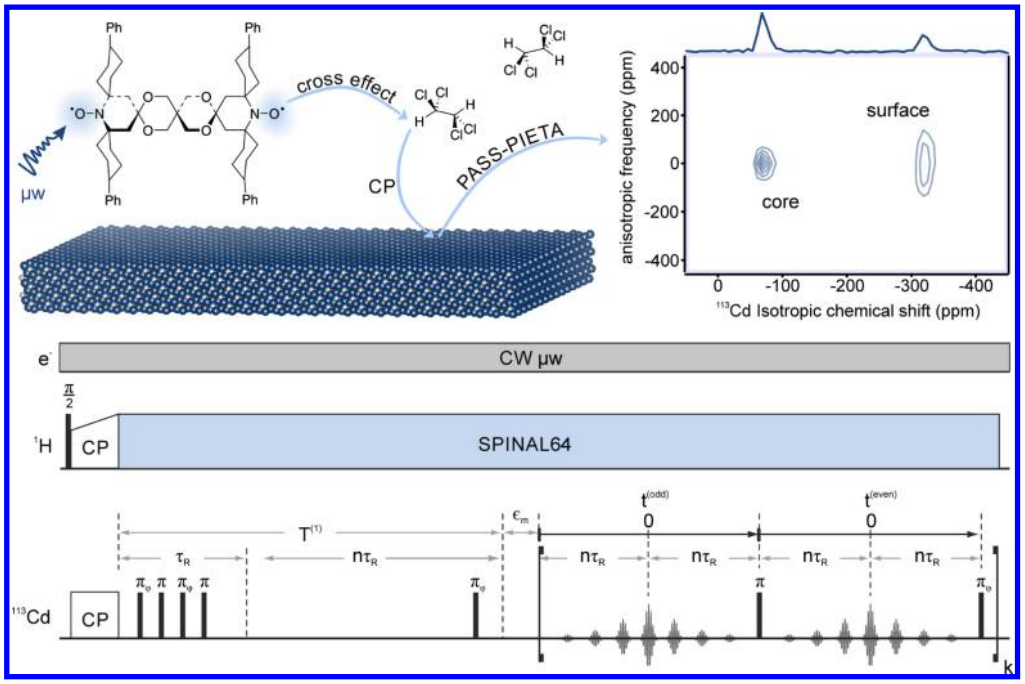

Figure 1. Scheme of the DNP enhanced PASS−PIETA experiment on NCs and its pulse sequence used in this work. DNP enhanced NMR makes use of the large polarization of unpaired electrons (top left) from radicals to enhance the NMR signal and to make complex NMR experiments, such as the acquisition of PASS−PIETA spectra (top right), feasible for low-concentration species. In cross-polarization-DNP (CP-DNP), continuous application of microwaves (CW μw) spontaneously hyperpolarizes the protons by the cross effect. TEKPol,[93] a well performing and established radical for DNP experiments, is depicted here as an example of a polarization source. A judicious choice for a solvent was 1,1,2,2-tetrachloroethane, which is highly suited for studying colloidal NCs with organic ligands, since it yields good DNP enhancement[94] and maintains colloidal stability of the NCs. From the protons, the hyperpolarization is then transferred to ^{113}Cd nuclei in the NCs by CP.[90,95] The obtained signal enhancements ($\varepsilon_{1_H} \approx 30-35$ at 14.1 T) at the surface or inside the NCs are large enough for informative but otherwise time-consuming NMR experiments to become feasible. In the pulse sequence shown here, the PASS pulse elements follow the CP step and retard the anisotropic chemical shift evolution at the end of the constant time block $T^{(1)}$ by an amount given by the parameter ε_m, which is controlled by the timings of the five hard π pulses within the block. The dependence of ε_m on these timings is governed by the Dixon's PASS equations.[70,71] The echo shift of $n\tau_R$ in between the fourth and fifth π pulses sets the length of the acquisition windows in between the refocusing π pulses of the echo train. The phase-incremented pulses are indicated by the symbol φ.

shell CdSe/CdS NCs with CdS coatings of various thicknesses. Likewise, pristine CdSe NPLs were compared to core/crown CdSe/CdS NPLs. Distinct DNP enhanced PASS−PIETA spectra are obtained of each of these structurally, morphologically, and compositionally different NCs. In particular, these spectra can capture small differences in the degree of the overall atomistic order (QDs versus NPLs, clusters versus QDs, etc.) as well as the differences in the surface termination (sulfide versus selenide). Surfaces of ZB polymorphs of CdSe QDs appear much less disordered than those of WZ counterparts. This study validates DNP enhanced PASS−PIETA NMR spectroscopy as a powerful characterization tool for inorganic nanostructures. Future avenues thus include the monitoring of the chemical transformations at the NC surface and core by, for instance, ligand-exchange and ion-exchange reactions, respectively.

RESULTS AND DISCUSSION

Our goal is to unravel the potential of DNP enhanced PASS−PIETA NMR spectroscopy for probing the atomistic structure of colloidal semiconductor NCs in their native colloidal state. As model systems, we have chosen the state-of-the-art long-chain-ligand-capped colloidal Cd-chalcogenide nanomaterials, synthesized by nonaqueous, high-temperature solution methods (at 240−360 °C): sub-10 nm ZB-CdSe NCs[84] and WZ-CdSe,[34] core/shell CdSe/CdS NCs,[85] magic-sized CdSe clusters,[86] pristine CdSe NPLs,[87,88] and core/crown CdSe/CdS NPLs.[89] For the subsequent studies, these NCs were maintained in a colloidal state using a solvent suitable for DNP experiments (1,1,2,2-tetrachloroethane). Such a methodology is thus readily applicable to all common ligand-capped colloidal NCs and requires only 1−2 mg of NCs dispersed in as little as 20−30 μL of the solvent. No crystal phase transition of CdSe is known to occur between room temperature (RT) and 100 K (DNP NMR experiment). In the following, we first outline the measurement methodology, and then discuss the results for each specific class of studied NCs.

DNP Enhanced PASS−PIETA NMR Spectroscopy of Colloidal NCs. The DNP enhanced PASS−PIETA experiment is schematically summarized in Figure 1: polarization is transferred from unpaired electron spins, whose transitions are saturated by monochromatic microwave, to protons of the solvent through the cross effect.[59] Signal enhancement of the nucleus of interest, such as ^{113}Cd, is then achieved by conventional cross-polarization (CP) from ^{1}H. The interaction enabling polarization transfer through CP is the dipolar interaction, whose distance-dependent coupling strength leads to a better polarization of the NC surface region than the core region, making the combination of DNP and CP a surface-enhanced NMR method.[62] All experiments described in this work are conducted with the CP step (thus the abbreviation CP is omitted for simplicity). If only CP were used for signal enhancement, conventional 2D PASS experiments would be prohibitively time-consuming[90] for the concentrations of NCs that are accessible to us. DNP provides sufficient signal

DOI: 10.1021/acscentsci.8b00196
ACS Cent. Sci. 2018, 4, 1113−1125

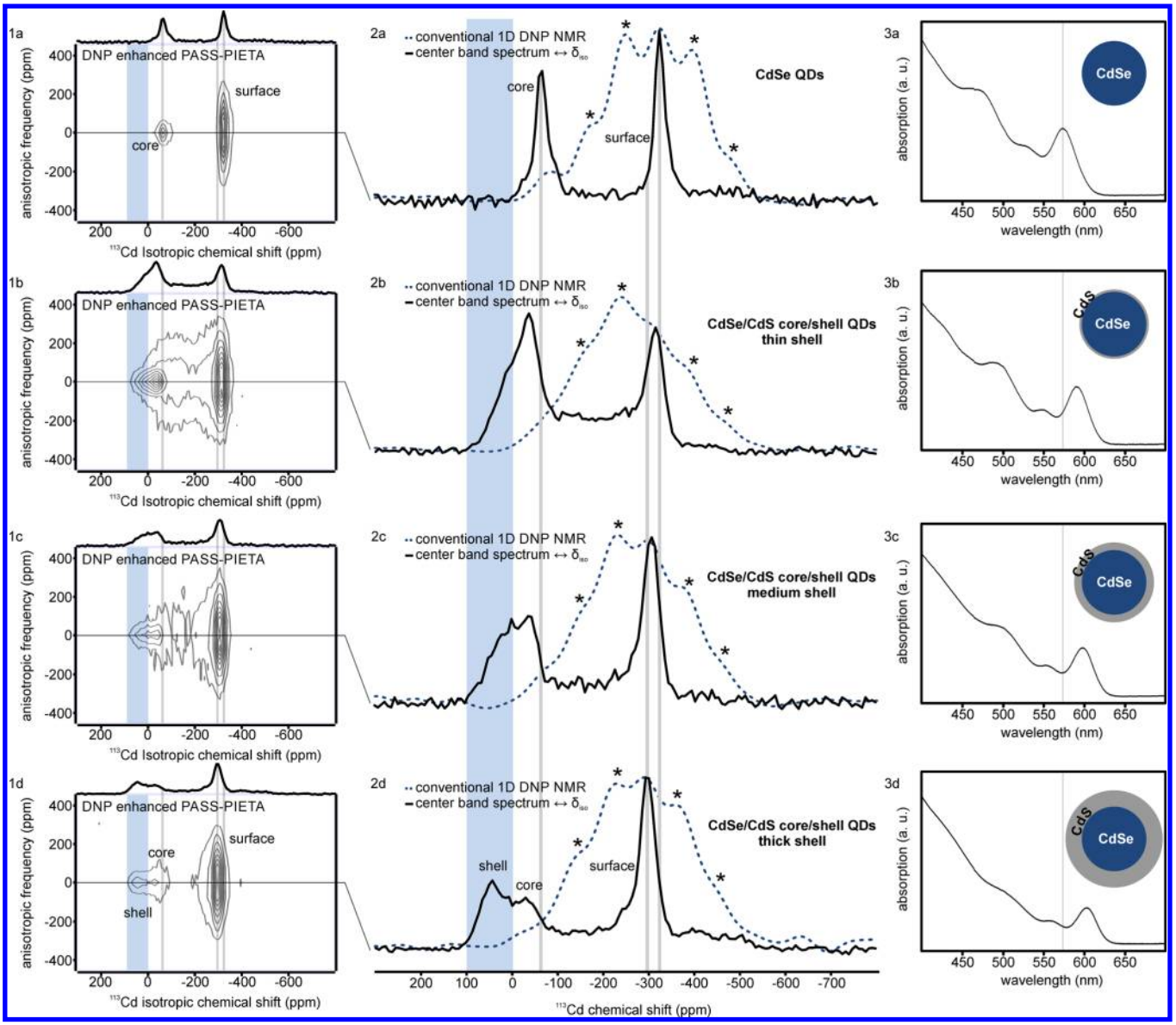

Figure 2. (1) DNP enhanced PASS−PIETA NMR spectra of (a) oleate-capped ZB-CdSe QDs on which a CdS shell of (b) 0.1 nm, (c) 0.4 nm, and (d) 0.9 nm thickness was grown. (3) Optical absorption spectra illustrate the gradual shift of the excitonic peak to lower energies with increasing shell thickness (reduced quantum confinement). The TEM images of these four QDs samples are shown in Figure S3. Insets in the absorption spectra are schematics of CdSe and CdSe/CdS core and core/shell QDs. The centerband spectra (solid black line in panels 2a−2d, corresponding to the zero frequency cross-sections in panels 1a−1d) show only isotropic chemical shift frequency components, providing qualitative information about the number and distribution of ^{113}Cd species present in the QDs. It is noted that centerband spectra, unlike full isotropic projections, are not generally quantitative, as the signal intensity of species giving large spinning sideband manifolds is reduced in comparison with the spectrum that one would obtain at infinite spinning speed. Information accessibility is strongly reduced in conventional 1D DNP NMR (dashed blue line in the panels 2a−2d). The surface, core and, if present, shell signals are specially labeled in panels 1a, 2a, 1d, and 2d. The signal assignments in panels 1b, 2b, 1c, and 2c have been omitted as they are very similar to signals from core CdSe and thick shell CdSe/CdS core/shell QDs. Spinning side bands are marked with asterisks.

enhancement of the colloidal NC surfaces to perform complex experiments such as D-HMQC[50] or, as proposed in this work, PASS−PIETA, yielding 2D spectra that clarify interactions, structures, and other spin-specific information that are not easily interpreted from 1D NMR spectra. The 2D PASS experiment[71] is used to separate and correlate the chemical shift signal components, allowing access not only to the high-resolution isotropic spectrum, but also to the size and distribution of the anisotropic components of the chemical shift tensor for distinct cadmium sites of the NC, resolved by their isotropic shifts. For the NC systems in this study, the inhomogeneous broadening of the isotropic resonances was generally sufficiently large and ^{113}Cd transverse coherence lifetimes suitably long to permit the collection of 60 full PASS−PIETA echoes of significant intensity, with the duty cycle of the proton decoupling ultimately limiting the number of echoes that could be collected. Under these conditions, the estimated sensitivity enhancement from multiple echo acquisition over conventional PASS is roughly a factor of 3.5. It is worth pointing out that, in each of the model systems investigated here, transverse coherence lifetimes are much longer than the sample rotation period. In such a limit, MAT−PIETA[71] is an equally valid choice of experiment.

DOI: 10.1021/acscentsci.8b00196
ACS Cent. Sci. 2018, 4, 1113−1125

Processing MAT−PIETA data entails a similar amount of effort as PASS−PIETA data, but the former pulse sequence may be easier to implement on some spectrometers. It is important to remember, however, that when transverse coherence lifetimes are comparable to or shorter than the sample rotation period, conventional 2D PASS will be the preferred sideband separation experiment.[71]

Altogether, we find our implementation of DNP enhanced PASS−PIETA improves the sensitivity of two-dimensional sideband separation experiments by roughly 2 orders of magnitude, enabling a high-throughput investigation of diverse high-surface-area materials, in the present case, cadmium-based NC systems. Herewith, the issue of overlapping signals is solved for NCs, where most of the spins are at or in close vicinity to the surface and experience highly anisotropic chemical and magnetic surroundings, leading to large CSAs. It is the higher spectral resolution due to PASS which enables (i) the identification of individual species, or of distributions of species, by their respective isotropic chemical shifts and (ii) the correlation of the spinning sideband manifolds to their respective isotropic chemical shifts. The CSA parameters of individual species can then be evaluated from the spinning sideband patterns, and compared to structural models obtained from density functional theory (DFT)[91] or Hartree−Fock theory.[92] Previously, such structural information was either inaccessible or involved elaborate first principle calculations. For example, Cadars et al. attempted determination of the chemical shifts of all ^{77}Se species within ZnSe NCs of different sizes, trying to reconstruct the observed spectra, without having the separate information on isotropic and anisotropic chemical shifts at hand.[55] Validation of such an analysis remains challenging since the contributions of the line-broadening effects such as site disorder or CSA oftentimes cannot be distinguished from one another in simple 1D NMR spectra with broad line widths. In summary, the DNP enhanced PASS−PIETA NMR experiment allows the number of different species, or their distribution, to be identified inside the sample (isotropic dimension, *x*-axis) and the species' surroundings (CSA-dimension, *y*-axis) to be determined.

Case of Oleate-Capped ZB-CdSe QDs. We begin our study by revisiting the oleate-capped ZB-CdSe QDs. The DNP surface-enhanced CP MAS NMR spectrum of nearly spherical oleate-capped ZB-CdSe QDs (e.g., 3.6 nm diameter, first absorption peak at 573 nm), a popular QD system, was reported in a previous investigation.[50] Two types of signals were observed in the ^{113}Cd spectrum: a narrow signal located at −60 ppm and a broad signal centered around −320 ppm. With the aid of a DNP enhanced ^{13}C−^{111}Cd-D-HMQC spectrum, the former type of signal was attributed to core cadmium atoms and the latter to cadmium oleate at the surface of the NC. The breadth of the surface signals had the appearance of a spinning sideband manifold, a consequence of large CSA due to the relatively asymmetric environment of the cadmium nuclei. In contrast, no significant spinning sidebands were observed for the signal corresponding to the cadmium in the core, thus indicating that the CSA for such sites is negligible, consistent with their isotropic, tetrahedral environment. Cadmium oleate (surface cadmium bound to oleate ligand) appears as the sole kind of cadmium species at the NC surface. The DNP enhanced PASS−PIETA experiments on the same oleate-capped ZB-CdSe QDs are in excellent agreement with the earlier assignments from ref 50 (Figure 2, panels 1a−3a): a signal with small CSA, i.e., with a symmetrical surrounding, was found at δ_{iso} = −66 ppm, and a signal with larger CSA, corresponding to an asymmetric surrounding such as for surface cadmium, was located at δ_{iso} = −323 ppm. By separating the anisotropic and isotropic contributions in a 2D spectrum using PASS the signals from the two cadmium species are well-separated and resolved (Figure 2, panel 1a), unlike in conventional 1D DNP NMR (blue dashed line in Figure 2, panel 2a). The centerband spectrum (black solid line in Figure 2, panel 2a) is the horizontal cross-section taken from the center of the ordinate of the double-sheared (TOP) processed 2D PASS−PIETA spectrum (Figure 2, panel 1a), and it shows dramatically improved spectral resolution (i.e., narrower, distinguishable signals) in comparison to the conventional 1D DNP NMR spectrum (very broad signal, blue dashed line in Figure 2, panel 2a). This demonstrates the advantage of sideband separation, as possible in PASS experiments. Spins with highly asymmetric and anisotropic chemical and electronic surroundings possess large CSA tensors and produce numerous, and in the case of NCs oftentimes overlapping, spinning sidebands in MAS NMR spectra. When one cannot suppress these spinning sidebands by faster spinning of the sample because of hardware limitations, conducting 2D PASS, or other sideband-separating experiments such as MAT, can yield a result equivalent to infinitely fast MAS. Such desired information, e.g., number, nature, and distribution of species, could be obtained by looking at the infinite speed spectrum of 2D PASS (projection along the indirect dimension) or the centerband spectrum. Additionally, the information contained in the CSA, i.e., asymmetry and anisotropy of the chemical surrounding of a spin, remains accessible for 2D PASS, which is not the case for spinning sideband suppression through fast MAS. The indirect dimension of 2D PASS corresponds to the sideband profile of the corresponding isotropic chemical shift and can be read out directly from the 2D PASS spectrum. The CSA parameters of a certain species can be extracted by fitting the slice of the 2D PASS spectrum at the corresponding isotropic chemical shift of the studied species. The fit results can then be correlated to actual chemical structures with the help of DFT.[91] Such a detailed analysis is in progress. Here, we opt instead for presenting a great utility, a qualitative interpretation of the CSA dimension.

Case of Oleate-Capped Core/Shell ZB-CdSe/CdS QDs. Oleate-capped ZB-CdSe QDs (Figure 2, panels 1a−3a) are overcoated by an epitaxial shell of CdS leading to an increase in NC diameter by 0.1 nm (Figure 2, panels 1b−3b), 0.4 nm (Figure 2, panels 1c−3c), and 0.9 nm (Figure 2, panels 1d−3d). The shell growth is monitored with optical absorption spectroscopy and TEM (Figure 2, panels 3a−3d and Figure S3). Growing a CdS shell affected ^{113}Cd NMR signals from both the surface and the core. Isotropic chemical shift values from the surface peaks all are in the region of around −310 ppm (Table 1 and Figure 2). A clear deshielding trend, from −323 to −297 ppm, is observed when increasing the CdS shell thickness. This correlates also with the bulk isotropic chemical shift, exhibiting similar deshielding behavior (−83 ppm for CdSe and 65 ppm for CdS).[46] Similar to the trend seen for the excitonic peak in the absorption spectrum, the shift of the core signal is greatest after the first step of growing a CdS shell. The CdS shell decreases the band gap of the QDs by reducing the confinement of electrons and better delocalizing them while the confinement for holes remains nearly unchanged. In the absorption spectra, the excitonic peak shifts thereby to the red (Figure 2, panels 3a−3d). Likewise, in the NMR spectra, the CdSe core signal in core/shell CdSe/CdS is deshielded to −37 ppm, compared to the core

DOI: 10.1021/acscentsci.8b00196
ACS Cent. Sci. 2018, 4, 1113−1125

Table 1. Isotropic Chemical Shift Values Observed for Various NCs Studied in This Work

NC type	shell (nm)	$\delta_{iso,core}$ [a] (ppm)[b]	$\delta_{iso,surface}$ [a] (ppm)[b]
oleate-capped CdSe QDs	0	−66	−323
oleate-capped core/shell CdSe/CdS QDs	0.1	16, −37	−316
oleate-capped core/shell CdSe/CdS QDs	0.4	24, −37	−308
oleate-capped core/shell CdSe/CdS QDs	0.9	53, −37	−297
oleate-capped CdSe NPLs	0	−62	−311
oleate-capped core/crown CdSe/CdS NPLs	0	57, −61	−281, −310
oleate-capped CdS QDs	0	52	−293

[a] $\delta_{iso,core}$ and $\delta_{iso,surface}$ indicate the isotropic chemical shifts of cadmium from the core and the surface of the NCs. [b] The resolution limit of the DNP enhanced PASS−PIETA NMR experiments was 7 ppm.

signal of the pristine CdSe QDs found at −66 ppm (Figure 2, panels 2a−2d and Table 1). Such correlations between chemical shift and overall electronic structure of NCs have been already reported previously.[43,45,55] The isotropic chemical shift of NCs was different for various particle sizes which was explained by the sensitivity of the chemical shift to the changes in the electronic structure of NCs (band gap width, absolute positions of the valence and conduction bands), caused by quantum-size effect.

While the CdSe core signal is deshielded with the growth of a CdS shell, a second signal is emerging as well, at higher frequencies. This second peak, attributed to the CdS shell, continues to rise in intensity and is further deshielded with increasing CdS shell thickness (Table 1 and Figure 2 panels 2b−2d). The CdS shell signal has an isotropic chemical shift similar to that of bulk CdS (65 ppm).[46] In a reference experiment with oleate-capped ZB-CdS QDs (Figure S4), the two signals attributed to the core (52 ppm) and the surface (−293 ppm, cadmium oleate) are in full agreement with the isotropic chemical shift values found for the shell in core/shell CdSe/CdS NCs.

Case of Oleate-Capped ZB-CdSe QDs versus ZB-CdSe NPLs. Comparing QDs and NPLs provided insight into the effect of NC shape and surface faceting. Surfaces of ZB-CdSe QDs consist of numerous crystal facets, edges, and corners, which are prone to dynamic rearrangements and defects. ZB-CdSe NPLs are unique in that their surfaces are atomically flat; namely, these are (001) facets.[87,96] CdSe platelets that are 4-monolayers thick (one layer = one Cd−Se distance), terminated with one additional cadmium layer, to which ligands bind, exhibit a thickness of 1.2 nm and a first absorption peak at 512 nm, in agreement with ref 97. In the DNP enhanced PASS−PIETA NMR spectra of these NPLs and ZB-CdSe QDs (3.0 nm diameter, first absorption peak at 547 nm), the signals from the cores are identical in isotropic and anisotropic chemical shifts within spectral resolution (Figure 3). This stands in expected agreement, because cadmium atoms in both types of particles have an identical highly symmetric tetrahedral environment of the ZB-lattice; in fact, also their optical band gaps are similar. On the contrary, the surface ^{113}Cd signals are measurably different: δ_{iso} = −311 ppm (NPLs) versus δ_{iso} = −323 ppm (QDs).

In NPLs, the CSA of the surface signal is just slightly larger than that of the core, highlighting the expected effect of the atomic flatness. On the contrary, the isotropic broadening of the surface signal of QDs is about twice as large compared to the surface signal of NPLs. In QDs, the surface curvature, edges, corners, and defects contribute to the increase of CSA of the QD surface signal. The core signals from both shapes have similar broadening in the isotropic dimension.

In the studied NPLs with dimensions (width1 × width2 × thickness) of (10−15) nm × (20−30) nm × 1.2 nm, at least 85% of the surface area is associated with (001) facets. The NPL surface signal at δ_{iso} = −311 ppm can thus be attributed to cadmium oleate on a (001) facet. Since ZB-CdSe QDs are mostly terminated with (001) and (111) facets,[98] one can hypothesize that the surface signal of QDs originates mainly from cadmium oleate on (001) and (111) facets. The (111)-related signal is found at δ_{iso} = −335 ppm after subtracting the (001) signal at −311 ppm. In QDs, additional factors—edges, surface defects, etc.—turn these two signals into a continuous distribution.

Case of Core/Crown CdSe/CdS NPLs. Core/crown NPLs (Figure 4) represent another recent addition to the family of complex NC heterostructures,[89,99,100] featuring enhanced optical properties such as greater photostability and higher photoluminescence quantum yield efficiency as compared to core-only CdSe NPLs. The band gap energy and the atomic order in the emissive CdSe core are largely unaffected by the

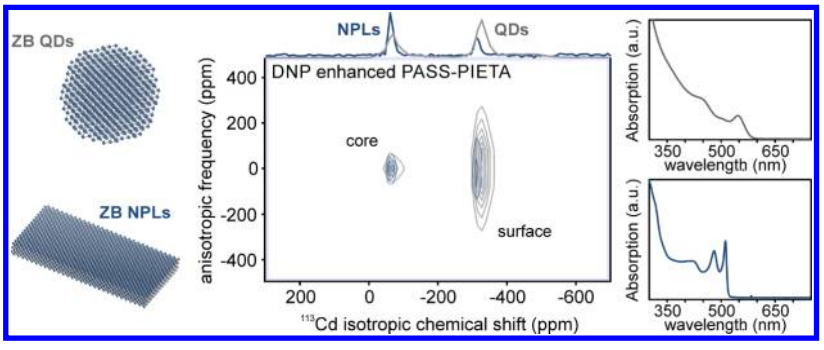

Figure 3. (left) Atomic models of cadmium-terminated ZB-CdSe QDs and NPLs are depicted. (middle) Superposition of oleate-capped ZB-CdSe NPLs (blue) and oleate-capped ZB-CdSe QDs (gray) DNP enhanced PASS−PIETA spectra. The core signals of NPLs and QDs are the same within the resolution limit of the PASS−PIETA experiment (Table 1). The surface signal of the NPLs is significantly narrower in the isotropic dimension and lies on the higher-frequency part of the QD surface signal. Most probably the QD signal is constituted of a signal from cadmium oleate on (001) facets (common with NPLs) and cadmium oleate on (111) facets (not overlapping with the NPL signal). Furthermore, QD signals exhibit a broader isotropic line width than NPLs indicating a larger diversity of sites and potentially disorder for QDs. (right) The absorption spectra show narrow excitonic peaks corresponding to monodisperse NC samples with similar absorption wavelength, i.e., similar band gaps.

DOI: 10.1021/acscentsci.8b00196
ACS Cent. Sci. 2018, 4, 1113−1125

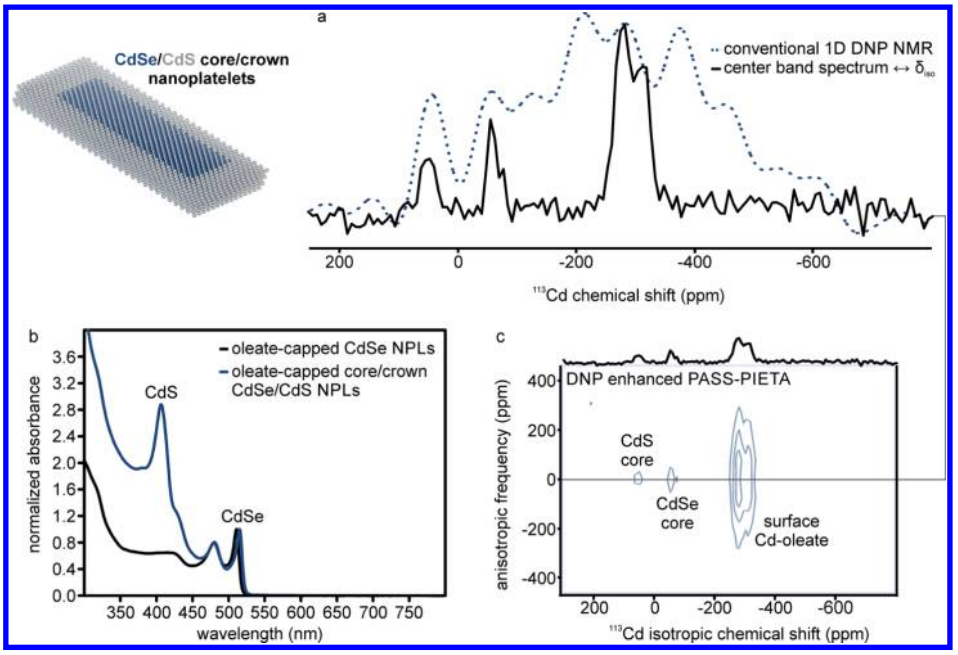

Figure 4. (left) In the top left corner, an atomic model of a cadmium-terminated core/shell CdSe/CdS NPL is depicted. From the conventional ^{113}Cd 1D DNP NMR spectrum of oleate-capped core/shell CdSe/CdS NPLs (blue dashed line in panel a), little information can be obtained because of large inhomogeneous broadening, including convolution of spinning sideband manifolds of surface species, causing extensive overlap of an unknown number of signals. The centerband spectrum (black solid line in panel a) of the DNP enhanced PASS−PIETA spectrum (panel c) shows only the isotropic chemical shift values with all spinning sidebands removed. Four cadmium species could be clearly resolved and assigned to cadmium in the CdS core (57 ppm) and in the CdSe core (−61 ppm), and to cadmium oleate at the surface of CdS (−281 ppm) and CdSe (−310 ppm). In the absorption spectrum (panel b), the excitonic peaks of the CdS and CdSe regions of the oleate-capped core/crown CdSe/CdS NPLs are clearly visible.

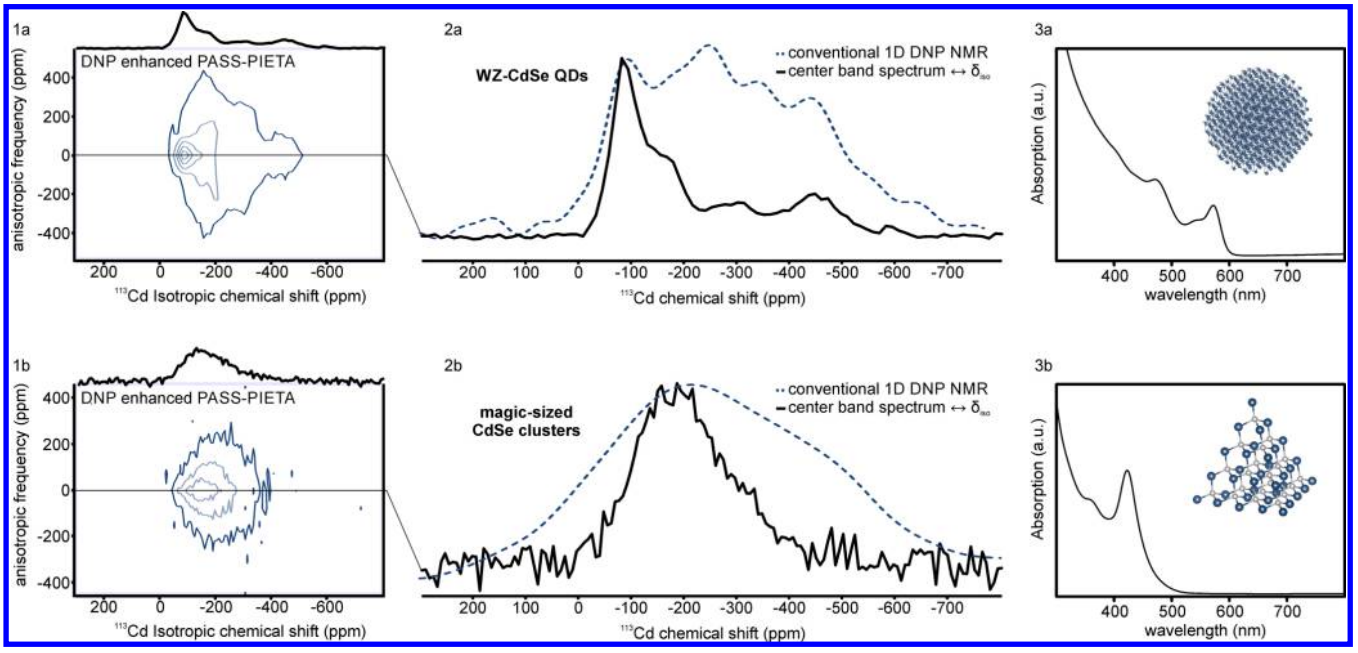

Figure 5. (1) DNP enhanced PASS−PIETA NMR spectra of (a) phosphonate-capped WZ-CdSe QDs and (b) benzoate-capped magic-sized CdSe clusters. The centerband spectra (black solid line in panels 2a and 2b) show only isotropic chemical shift frequency components, providing information about the number and distribution of ^{113}Cd species present in the WZ-QDs and in sub-2 nm CdSe clusters. This information was not accessible with conventional 1D DNP NMR (dashed blue line in panels 2a and 2b). (3) Absorption spectra of the colloidal dispersions of both kinds of CdSe species. The insets in the absorption spectra are schematics of a WZ-CdSe QD (3a) and a possible structure for magic-sized CdSe clusters (3b), as suggested on the basis of a pair-distribution-function study.[106]

CdS crown. The peculiar core/crown morphology has been thoroughly characterized with TEM, elemental mapping, and optical spectroscopy (Figure S5 and the literature[89,99,100]). CdSe core and CdS crown have identical thickness.

Conventional ^{113}Cd 1D DNP NMR yields only a broad spectrum (dashed blue line in Figure 4a), and unambiguous assignment of the core and surface signals of CdSe and CdS regions is rather impossible. On the contrary, the DNP

DOI: 10.1021/acscentsci.8b00196
ACS Cent. Sci. 2018, 4, 1113−1125

enhanced PASS−PIETA NMR spectrum of such NPLs (Figure 4c, centerband spectrum, black solid line in Figure 4a) allows for a needed insight: four peaks are identified at 57, −61, −281, and −310 ppm. The first two exhibit very small CSAs, are well-resolved, and can each be, respectively, attributed to core CdS and core CdSe peaks, based on their isotropic chemical shifts (Table 1). The CdSe core signal at −61 ppm closely matches the pristine CdSe NPLs (−62 ppm, Table 1). The signal at 57 ppm can be assigned to the core of CdS crown, consistent with the general trend of the isotropic chemical shift values of bulk CdE (E = S, Se, Te) shifting to lower frequencies for heavier chalcogenides.[46] Isotropic chemical shift of ZB-CdS QDs peaks at 52 ppm (Figure S4). The literature value for bulk CdS is also closely located (65 ppm).[46] The surface-related signals at −281 and −310 ppm are assigned to CdS and CdSe regions, respectively. A relatively small chemical shift difference for surface signals (in comparison to core regions) correlates with the expectation that surface Cd atoms are in joint coordination with oleate ligands, and the chalcogenides constitute only approximately half of the coordination sphere.

The fact that CdSe-related isotropic chemical shifts of the core and the surface are nearly identical to those of pristine CdSe NPLs confirms that the CdS crown grew exclusively by lateral extension of the platelet, without concomitant deposition of CdS onto the large (001) facets. Furthermore, the surface species on the CdSe and the CdS regions are apparently of the same identity (Cd-oleates). Further support to this conclusion comes from the optical absorption spectra, where the first absorption peak of CdSe is only slightly red-shifted by ca. 4 nm (Figure S5), indicating the preservation of strong quantum confinement. Conversely, growing a CdS shell onto CdSe NPLs of the same thickness reportedly causes a shift of at least 60 nm to the red after adding just one monolayer of CdS.[88,97,100−102]

Effect of the Core Crystal Structure. Thus far, the crystal structures of all discussed NC systems were of ZB-type. For an illustration of the effect of the crystal structure, Figure 5 presents NMR spectra from WZ-CdSe QDs (3.6 nm diameter, sub-10% standard size-deviation, first absorption peak at 572 nm) and magic-sized CdSe clusters (1st absorption peak at 423 nm, sub-2 nm size). Importantly, direct comparison of ZB versus WZ crystal structure cannot be carried out with bulk references, because bulk CdSe crystallizes exclusively in a WZ polymorph.

The DNP enhanced PASS−PIETA NMR spectrum of WZ-CdSe QDs exhibits more than two signals, covering a broad distribution of isotropic chemical shift values (Figure 5, panel 1a; centerband spectrum, black solid line in panel 2a), making clearly evident a far greater atomistic complexity compared to ZB-CdSe QDs (Figure 2). Our interpretation is that the signal at −80 ppm, which cannot be observed in the conventional 1D DNP NMR spectrum (blue dashed line in Figure 5, panel 2a), corresponds to the core signal, which is relatively close to the −66 ppm found for the core of ZB-CdSe QDs. The remaining signals in WZ-CdSe QDs can be attributed to various surface cadmium atoms. Indeed, the faceting of the hexagonal crystal structure is expected to be more complex,[103,104] including the existence of polar terminations (Cd or Se terminations of opposite facets).[105] Further, the capping ligands of the studied WZ-CdSe QDs are phosphonate molecules and not oleate as for ZB-CdSe. This complexity is rather hidden in optical absorption and emission spectra, wherein both crystal polymorphs feature identically sharp excitonic bands (absorption spectra of ZB-CdSe QDs Figure 2, panel 3a and Figure 3 top right; absorption spectrum of WZ-CdSe QDs Figure 5, panel 3a).

In the case of magic-sized CdSe clusters, prepared according to ref 86, the crystal structure differs from both polymorphs and is not precisely known. It could be described as a molecular structure with very limited periodicity in atomic positions. Hence, every single atom is expected to engender a signal at a different isotropic chemical shift value. This provides a plausible explanation of the striking broadness of the featureless centerband spectrum (black solid line in Figure 5, panel 2b). By removing the spinning sidebands, this spectrum is significantly narrower than a conventional 1D DNP NMR spectrum (blue dashed line in Figure 5, panel 2b). The remaining inhomogeneous broadening is ascribed to the site disorder, i.e., a continuous distribution of ^{113}Cd isotropic chemical shift values, in a manner similar to that observed in glassy materials. Analogously, it may be possible to use the information content of the CSA to accurately quantify distributions[107,108] of Se−Cd−Se bond angles and Cd−Se bond lengths and perhaps even their electronic and optical properties. Future work along these lines is in progress.

EXPERIMENTAL SECTION

Materials. Benzoic acid (Brunschwig AG), cadmium acetate dihydrate ($Cd(OAc)_2{\cdot}2H_2O$, Fluka, ≥98%), cadmium nitrate tetrahydrate ($Cd(NO_3{\cdot}4H_2O)_2$, Fluka, ≥99%), cadmium oxide (CdO, Armar Chemicals, >99.99%), diphenylphosphine (DPP, Aldrich, 98%), dodecylamine (Aldrich, 98%), 1-octadecene (ODE, Aldrich, 90%), *n*-octadecylphosphonic acid (ODPA, PCI Synthesis), octylamine (Aldrich), oleic acid (OA, Aldrich, 90%), oleylamine (OLA, Aldrich, 70%), selenium (Se, Aldrich, 100 mesh, 99.99%), selenium dioxide (SeO_2, Strem, 99.8%), sodium myristate (Na(myr), TCI, ≥98%), sulfur (S, Aldrich, 99.998%), trioctylphosphine (TOP, 97%, Strem), and trioctylphosphine oxide (TOPO, ACROS or Aldrich, 99%) were used. All materials were used without further purification. The solvents ethanol (EtOH), hexane, methanol (MeOH), and toluene as well as anhydrous acetone, acetonitrile, ethanol, hexane, and toluene were obtained from various sources (Aldrich, VWR, Merck). The biradical polarizing agent TEKPol[109] was provided by Dr. Olivier Ouari, Dr. Gilles Casano, and Prof. Dr. Paul Tordo (Aix-Marseille Université). The meso-SiO_2 matrices hexagonal mesostructured silica (MSU-H, 7 nm pore size, Aldrich cat. 643637), silica gel (Davisil grade 643, 15 nm pore size, Aldrich cat. 236810), and silica gel (spherical shapes, 30 nm pore size, AlfaAesar cat. 44101) were used as supplied. Cadmium is a toxic heavy metal, and handling of cadmium-containing chemicals and NCs should be done with appropriate safety precautions.

Cd and S Precursors. Cadmium myristate, $Cd(myr)_2$, was synthesized following a procedure from the literature,[84] i.e., by dropwise addition of 3.1 g of $Cd(NO_3)_2{\cdot}4H_2O$ (10 mmol) in 100 mL of MeOH to 7.5 g of Na(myr) (30 mmol) in 1 L of MeOH. Precipitated $Cd(myr)_2$ was filtrated, washed twice with MeOH, and dried in a vacuum oven at 50 °C for 16 h. Cadmium oleate in 30 mL of ODE (0.1 M) was prepared using 0.544 g of CdO (4 mmol) and 7.5 mL of OA (21 mmol). The mixture was degassed for 10 min at RT and subsequently heated to 240 °C under argon until the solution became colorless. The mixture was then cooled down to 100 °C and dried for 1 h under vacuum. The S-ODE precursor (0.1 M) was prepared by adding 0.096 g of S (3 mmol) into 30 mL of ODE, heated up to 160 °C under argon, and then cooled down to 100 °C and dried for 1 h.

Oleate-Capped ZB-CdSe QDs. Oleate-capped ZB-CdSe QDs of 3.0 and 3.6 nm diameter (determined from absorption

DOI: 10.1021/acscentsci.8b00196
ACS Cent. Sci. 2018, 4, 1113−1125

spectra) were synthesized following a literature method, with minor modifications.[84] In a typical synthesis, 115 mg of CdO (1 mmol) and 1.5 mL of OA (4 mmol) were mixed with 15 mL of dried ODE in a 100 mL three-neck flask and degassed for 10 min at RT. The mixture was then heated under nitrogen to 240 °C until the solution became colorless. After cooling to 100 °C, the solution was evacuated for 1 h and then cooled to RT. A 0.1 g portion of SeO_2 (1 mmol) was added under nitrogen flow, and the mixture was heated to 240 °C at a rate of 20 °C/min. After 3 min at 230 °C, or 240 °C for the larger QDs, the crude solution was cooled down to RT. CdSe QDs were washed three times with hexane and EtOH. After purification, CdSe QDs were dispersed in hexane for NMR experiments or for the growth of CdSe/CdS core/shell NCs. Powder X-ray diffraction (PXRD) patterns are shown in Figures S1 and S2 and the absorption spectra in Figures 2 and 3. QD sizes determined from the TEM images (Figure S1) were found to be 2.9 nm (15% size distribution) and 3.7 nm (11% size distribution).

Oleate-Capped CdSe/CdS Core/Shell QDs. Oleate-capped CdSe/CdS core/shell QDs were prepared by growing a CdS shell onto oleate-capped ZB-CdSe QDs by successive ion layer adsorption and reaction (SILAR).[85] The precursors for the alternative injections, cadmium oleate and S-ODE, were prepared in advance, as described above, and stored under argon. A 100 mL flask was loaded with 40 mg of oleate-capped ZB-CdSe QDs [3.6 nm diameter size by absorption, 3.7 nm (11% size distribution) from TEM images] dissolved in 1 mL of hexane, 2 mL of OLA, and 5 mL of ODE. The mixture was kept for 1 h under vacuum at 100 °C. After switching to argon, 0.1 M cadmium oleate was injected, and the temperature was increased to 240 °C. After 10 min, the S-ODE precursor was injected. Successive injections of alternatively cadmium and sulfur precursors had been carried out every 10 min until precursor quantities for 4, 7, and 10 layers of CdS were converted (0.1, 0.4, and 0.9 nm shell thickness with size distributions of 13%, 14%, and 13%, respectively, were obtained as estimated from TEM images in Figure S3). Simple geometric calculation defines the quantities of Cd and S precursors: the first injection of precursors with 0.1 M concentration was 0.25 mL, followed by 0.34 mL up to 1.67 mL for a 10th layer. After the last injection, the flask was cooled to RT, and the NCs were purified with toluene and EtOH three times. PXRD patterns are reported in Figure S2, and the absorption spectra are found in Figure 2.

Oleate-Capped ZB-CdSe NPLs. Oleate-capped ZB-CdSe NPLs with emission peak centered at 512 nm were synthesized as reported elsewhere,[87,88] with slight modifications. A 222 mg portion of $Cd(myr)_2$ (0.4 mmol), 15.7 mg of Se powder (0.2 mmol), and 20 mL of ODE were degassed in a three-neck flask at RT for 30 min and heated up to 100 °C under vacuum. Then, the flask was filled with argon, and the mixture was quickly heated to 240 °C. When the temperature reached 190−195 °C, 52 mg of $Cd(OAc)_2{\cdot}2H_2O$ (0.2 mmol) was introduced as a powder together with 1 mL of hexane under argon. The reaction mixture was kept at 235−240 °C for 5 min and cooled to RT, adding 2.6 mL of OA and 3 mL of hexane while at 65−70 °C. NPLs were separated by centrifuging and redispersed in 4.5 mL of hexane, mixed with 2.5 mL of EtOH, and centrifuged again. NPLs were then dispersed in 1 mL of hexane and filtered through a 0.45 μm PTFE filter. For characterization of the NPLs, TEM, PXRD (both Figure S1), and absorption spectrum (Figure 3) were acquired.

Oleate-Capped CdSe/CdS Core/Crown NPLs. Oleate-capped CdSe/CdS core/crown NPLs of large size were synthesized as described elsewhere[89] with some modifications. $Cd(OAc)_2{\cdot}2H_2O$ (480 mg, 1.8 mmol), OA (340 μL, 1 mmol), and ODE (2 mL) were mixed and heated to 150 °C for 12 h while stirring under air. A 3 mL portion of 0.1 M S solution in ODE was added, and the obtained dispersion, the anisotropic growth mixture, was kept stirring until injection. Core CdSe NPLs were synthesized as described above but were not purified. The entire product of a CdSe NPLs synthesis (∼25 mg of unwashed NPLs) was mixed with 3.3 mL of ODE in a three-neck flask, degassed for 20 min, and heated to 240 °C under argon for 10 min. A 3.3 mL portion of the anisotropic growth mixture was then injected with a syringe pump at a rate of 8 mL/h maintaining reaction temperatures of 240 °C. The obtained CdSe/CdS core/crown NPLs were precipitated with EtOH and dispersed in hexane. Full characterization is shown in Figure S5.

Phosphonate-Capped WZ-CdSe QDs. Phosphonate-capped WZ-CdSe QDs of 3.6 nm in diameter (by absorption spectroscopy, see Figure 5) were prepared according to Bawendi et al.[34] A 60 mg portion of CdO (0.467 mmol), 282 mg of ODPA (0.843 mmol), and 3 g of TOPO (7.798 mmol) were dried under vacuum for 1 h at 150 °C. The mixture was heated to 230 °C under nitrogen flow until a transparent colorless solution was obtained, and further heated to 320 °C, at which point 1 mL of TOP was added. At 360 °C, TOP-Se solution (61 mg, 0.772 mmol of Se in 500 μL of TOP) was swiftly injected, and the heating mantle was removed. After 90 s, the reaction mixture was quickly cooled down to RT. A 5 mL portion of anhydrous toluene was added during cooling to prevent TOPO from solidifying. The QDs were washed using a toluene/EtOH solvent/antisolvent system. Small quantities of octylamine were used to facilitate purification of the QDs. TEM images in Figure S6 yielded an average particle size of 4.0 nm (13% size distributions). PXRD is shown in Figure S6.

Benzoate-Capped CdSe Magic-Sized Clusters. Benzoate-capped CdSe magic-sized clusters with an absorption peak at 423 nm were synthesized according to the procedure of Cossairt et al.,[86] with minor modifications. A 310 mg portion of selenium (3.9 mmol) was dissolved in 730 μL of DPP (4.2 mmol) and 10 mL of anhydrous toluene inside the glovebox. A 25 mL three-neck flask was loaded with 0.5 g of CdO (3.9 mmol), 1.5 g of benzoic acid (12.3 mmol), and 2.0 g of dodecylamine (10.8 mmol). The Cd-benzoate was dried at 110 °C for several hours under vacuum and was then heated to 210 °C under nitrogen for 10 min until the mixture had become a colorless solution. The temperature of the reaction flask was reduced to 110 °C and degassed again under vacuum. After 40 min, the temperature was reduced to 55 °C. DPP-Se solution was injected, and the reaction was stirred for 170 min. The reaction mixture was dried using vacuum distillation and transferred into the glovebox, followed by the addition of 10 mL of anhydrous hexane. The resulting suspension was centrifuged (at RT); the supernatant was stored in the freezer for 3 days and centrifuged again (at 5 °C). The new supernatant was dried. The resulting solid of CdSe clusters was purified twice by dissolving in 15 mL of anhydrous toluene, adding 30 mL of anhydrous acetonitrile, and centrifuging, and was stored airless in an anhydrous toluene solution. The absorption spectrum is displayed in Figure 5.

DNP NMR Experiments. DNP NMR spectra were acquired at about 100 K using a Bruker Avance III spectrometer operating at 14.1 T and a 395 GHz gyrotron microwave source with an output power of approximately 6 W.[110] The 3.2 mm HX and HXY low-temperature MAS probes were used with sapphire

DOI: 10.1021/acscentsci.8b00196
ACS Cent. Sci. 2018, 4, 1113−1125

rotors.[110] CP transfer[90,95] was conducted with ramped contact.[111] Delay times were set to be 1.3 times the T_1 obtained from saturation recovery experiments of the protons of the solvent. The SPINAL-64 heteronuclear decoupling sequence[112] with a radio frequency field of 100 kHz was used for all DNP NMR experiments. Chemical shifts were referenced to Me_2Cd (^{113}Cd). Detailed experimental conditions such as pulse sequence, spinning frequency of the MAS, pulse length, etc. for each NMR experiment are listed in the Supporting Information.

DNP Enhanced Phase Adjusted Spinning Sidebands with Phase-Incremented Echo-Train Acquistion (PASS−PIETA). The direct excitation version of PASS−PIETA[71] is adapted for DNP by replacing the ^{113}Cd excitation pulse with $^{1}H \rightarrow {}^{113}Cd$ CP in the presence of microwave irradiation, as depicted in Figure 1. After this process generates hyperpolarized ^{113}Cd transverse magnetization, PASS signal is prepared by the application of five hard π pulses over a constant time interval $T^{(1)}$ to retard the CSA evolution by ε_m while leaving the isotropic chemical shift evolution unchanged at the end of the interval. The indirect dimension of the experiment completely samples the CSA evolution over one rotor period t_R, and the number of steps taken to advance ε_m over this interval determines the size of the spectral window of this dimension. On the basis of the number of samples taken in the indirect dimension, the pulse sequence automatically calculates the five π pulse timings for the desired number of samples in the indirect dimension based on a lookup table giving the solutions of the Dixon equations for 1024-step 2D PASS.[70] To adapt PASS for multiple echo acquisition, an echo shift equal to an integer multiple of the rotor period is included between the fourth and fifth π pulses in the constant time block. Obtaining a valid signal for both odd and even echoes requires delaying the onset of echo-train acquisition after $T^{(1)}$ by ε_m, and all sets of echoes must each be processed using different double-shear (TOP) transformations to separate and correlate the anisotropic and isotropic signal components.[76] In PASS−PIETA, the signal is also acquired as a function of a pulse phase parameter at a constant receiver phase, allowing the symmetry pathways carrying artifactual PASS signals to be eliminated by a few simple additional signal processing steps instead of complicated phase cycling schemes.[75,76]

DNP NMR Sample Preparation. DNP NMR sample preparation was performed using meso-SiO_2 as reported previously:[50] a highly concentrated colloidal NC solution was mixed with a solution of the organic biradical TEKPol in 1,1,2,2-tetrachloroethane[94,109] to yield a homogeneous solution which is impregnated with a minimal amount of meso-SiO_2 of optimal pore size before being packed into a sapphire rotor. The interested reader is referred to the Supporting Information for further details on sample preparation for each individual experiment.

CONCLUSION AND OUTLOOK

An NMR toolbox for characterizing inorganic nanostructures that significantly improves NMR resolution (2D PASS) with efficient sensitivity enhancement methods (DNP, PIETA) is presented. Two-dimensional PASS resolves the limitations related to the separation of overlapping sideband signals caused by large CSA, a typical case for nanomaterials. The combined method, called DNP enhanced PASS−PIETA, has been showcased and validated for structural characterization of colloidal semiconductor Cd chalcogenide NCs with high structural and compositional complexities. Such NMR studies can be conducted on NC samples that retain a pristine colloidal state, without invasive sample preparation. Because of the 100-fold improvement in NMR sensitivity, well-resolved NMR spectra can be obtained from small quantities of nanomaterials (1−2 mg). All observed ^{113}Cd NMR signals were confidently assigned to NC cores and surfaces, as well as to CdSe and CdS regions, and some first suggestive attempts were undertaken to assign crystal facets of ZB-CdSe NCs. DNP enhanced PASS−PIETA spectra enabled us to track the evolution of the isotropic chemical shift signals upon formation of CdSe/CdS nano-heterostructures (core/shell NCs or core/crown NPLs). A large decrease in the atomic order has been detected between ZB-CdSe nanostructures and WZ-CdSe QDs or magic-sized CdSe clusters. Future work will focus on signal assignments and analysis of CSA tensor parameters with the aid of DFT simulations.

ASSOCIATED CONTENT

Supporting Information

The Supporting Information is available free of charge on the ACS Publications website at DOI: 10.1021/acscentsci.8b00196.

Additional figures including TEM images, PXRD patterns, NMR spectra, and STEM images (PDF)

AUTHOR INFORMATION

Corresponding Authors

*E-mail: ccoperet@ethz.ch.
*E-mail: mvkovalenko@ethz.ch.

ORCID

Dmitry N. Dirin: 0000-0002-5187-4555
Loredana Protesescu: 0000-0002-9776-9881
Norberto Masciocchi: 0000-0001-9921-2350
Antonietta Guagliardi: 0000-0001-6390-2114
Lyndon Emsley: 0000-0003-1360-2572
Christophe Copéret: 0000-0001-9660-3890
Maksym V. Kovalenko: 0000-0002-6396-8938

Present Addresses

[#]T.-C. Ong: Department of Chemistry and Biochemistry, University of California Los Angeles, Los Angeles, California 90095, United States.
[▽]L. Protesescu: Department of Chemistry, Massachusetts Institute of Technology, 77 Massachusetts Avenue, Cambridge, Massachusetts 02139, United States.

Author Contributions

The manuscript was prepared through the contribution of all authors.

Notes

The authors declare no competing financial interest.

ACKNOWLEDGMENTS

M. V. Kovalenko acknowledges financial support from the European Union through the FP7 (ERC Starting Grant NANOSOLID, GA 306733), L. Emsley acknowledges support from ERC Advanced Grant 320860, L. Piveteau acknowledges financial support from Scholarship Fund of the Swiss Chemical Industry (SSCI Award 2015). René Verel is acknowledged for his help at the NMR facility at ETH Zurich. Electron microscopy was conducted at the Scientific Center for Optical and Electron Microscopy (ScopeM) and at Empa Electron Microscopy Center. Alla Sologubenko, Maryna Bodnarchuk, and Bogdan M.

DOI: 10.1021/acscentsci.8b00196
ACS Cent. Sci. 2018, 4, 1113−1125

Benin are acknowledged for taking TEM images and for elemental mapping using EDX.

REFERENCES

(1) Talapin, D. V.; Lee, J.-S.; Kovalenko, M. V.; Shevchenko, E. V. Prospects of Colloidal Nanocrystals for Electronic and Optoelectronic Applications. *Chem. Rev.* **2010**, *110*, 389−458.

(2) Protesescu, L.; Yakunin, S.; Bodnarchuk, M. I.; Krieg, F.; Caputo, R.; Hendon, C. H.; Yang, R. X.; Walsh, A.; Kovalenko, M. V. Nanocrystals of cesium lead halide perovskites ($CsPbX_3$, X = Cl, Br, and I): novel optoelectronic materials showing bright emission with wide color gamut. *Nano Lett.* **2015**, *15*, 3692−3696.

(3) Biju, V. Chemical Modifications and Bioconjugate Reactions of Nanomaterials for Sensing, Imaging, Drug Delivery and Therapy. *Chem. Soc. Rev.* **2014**, *43*, 744−764.

(4) Bertolotti, F.; Dirin, D. N.; Ibanez, M.; Krumeich, F.; Cervellino, A.; Frison, R.; Voznyy, O.; Sargent, E. H.; Kovalenko, M. V.; Guagliardi, A.; Masciocchi, N. Crystal Symmetry Breaking and Vacancies in Colloidal Lead Chalcogenide Quantum Dots. *Nat. Mater.* **2016**, *15*, 987−994.

(5) Boles, M. A.; Ling, D.; Hyeon, T.; Talapin, D. V. The Surface Science of Nanocrystals. *Nat. Mater.* **2016**, *15*, 141−364.

(6) Wang, R.; Shang, Y.; Kanjanaboos, P.; Zhou, W.; Ning, Z.; Sargent, E. H. Colloidal Quantum Dot Ligand Engineering for High Performance Solar Cells. *Energy Environ. Sci.* **2016**, *9*, 1130−1143.

(7) Houtepen, A. J.; Hens, Z.; Owen, J. S.; Infante, I. On the Origin of Surface Traps in Colloidal II−VI Semiconductor Nanocrystals. *Chem. Mater.* **2017**, *29*, 752−761.

(8) Owen, J. The Coordination Chemistry of Nanocrystal Surfaces. *Science* **2015**, *347*, 615−616.

(9) Konstantatos, G.; Howard, I.; Fischer, A.; Hoogland, S.; Clifford, J.; Klem, E.; Levina, L.; Sargent, E. H. Ultrasensitive Solution-Cast Quantum Dot Photodetectors. *Nature* **2006**, *442*, 180−183.

(10) Tang, J.; Kemp, K. W.; Hoogland, S.; Jeong, K. S.; Liu, H.; Levina, L.; Furukawa, M.; Wang, X.; Debnath, R.; Cha, D.; Chou, K. W.; Fischer, A.; Amassian, A.; Asbury, J. B.; Sargent, E. H. Colloidal-Quantum-Dot Photovoltaics using Atomic-Ligand Passivation. *Nat. Mater.* **2011**, *10*, 765−771.

(11) Yakunin, S.; Dirin, D. N.; Protesescu, L.; Sytnyk, M.; Tollabimazraehno, S.; Humer, M.; Hackl, F.; Fromherz, T.; Bodnarchuk, M. I.; Kovalenko, M. V.; Heiss, W. High Infrared Photoconductivity in Films of Arsenic-Sulfide-Encapsulated Lead-Sulfide Nanocrystals. *ACS Nano* **2014**, *8*, 12883−12894.

(12) Shulga, A. G.; Derenskyi, V.; Salazar-Rios, J. M.; Dirin, D. N.; Fritsch, M.; Kovalenko, M. V.; Scherf, U.; Loi, M. A. An All-Solution-Based Hybrid CMOS-Like Quantum Dot/Carbon Nanotube Inverter. *Adv. Mater.* **2017**, *29*, 1701764.

(13) Kagan, C. R.; Murray, C. B. Charge Transport in Strongly Coupled Quantum Dot Solids. *Nat. Nanotechnol.* **2015**, *10*, 1013−1026.

(14) Kagan, C. R.; Lifshitz, E.; Sargent, E. H.; Talapin, D. V. Building Devices from Colloidal Quantum Dots. *Science* **2016**, *353*, 55231−55239.

(15) Choi, J.-H.; Wang, H.; Oh, S. J.; Paik, T.; Sung, P.; Sung, J.; Ye, X.; Zhao, T.; Diroll, B. T.; Murray, C. B.; Kagan, C. R. Exploiting the Colloidal Nanocrystal Library to Construct Electronic Devices. *Science* **2016**, *352*, 205−208.

(16) Lee, J.-S.; Kovalenko, M. V.; Huang, J.; Chung, D. S.; Talapin, D. V. Band-Like Transport, High Electron Mobility and High Photoconductivity in All-Inorganic Nanocrystal Arrays. *Nat. Nanotechnol.* **2011**, *6*, 348−352.

(17) Thompson, N. J.; Wilson, M. W. B.; Congreve, D. N.; Brown, P. R.; Scherer, J. M.; Bischof; Thomas, S.; Wu, M.; Geva, N.; Welborn, M.; Voorhis, T. V.; Bulović, V.; Bawendi, M. G.; Baldo; Marc, A. Energy Harvesting of Non-Emissive Triplet Excitons in Tetracene by Emissive PbS Nanocrystals. *Nat. Mater.* **2014**, *13*, 1039−1043.

(18) Chuang, C.-H. M.; Brown, P. R.; Bulović, V.; Bawendi, M. G. Improved Performance and Stability in Quantum Dot Solar Cells Through Band Alignment Engineering. *Nat. Mater.* **2014**, *13*, 796−801.

(19) Speirs, M. J.; Dirin, D. N.; Abdu-Aguye, M.; Balazs, D. M.; Kovalenko, M. V.; Loi, M. A. Temperature Dependent Behaviour of Lead Sulfide Quantum Dot Solar Cells and Films. *Energy Environ. Sci.* **2016**, *9*, 2916−2924.

(20) Yuan, M.; Liu, M.; Sargent, E. H. Colloidal Quantum Dot Solids for Solution-Processed Solar Cells. *Nat. Energy* **2016**, *1*, 16016.

(21) Pietryga, J. M.; Park, Y.-S.; Lim, J.; Fidler, A. F.; Bae, W. K.; Brovelli, S.; Klimov, V. I. Spectroscopic and Device Aspects of Nanocrystal Quantum Dots. *Chem. Rev.* **2016**, *116*, 10513−10622.

(22) Saran, R.; Curry, R. J. Lead Sulphide Nanocrystal Photodetector Technologies. *Nat. Photonics* **2016**, *10*, 81−92.

(23) Owen, J.; Brus, L. Chemical Synthesis and Luminescence Applications of Colloidal Semiconductor Quantum Dots. *J. Am. Chem. Soc.* **2017**, *139*, 10939−10943.

(24) García de Arquer, F. P.; Armin, A.; Meredith, P.; Sargent, E. H. Solution-Processed Semiconductors for Next-Generation Photodetectors. *Nat. Rev. Mater.* **2017**, *2*, 16100.

(25) Yang, Z.; Fan, J. Z.; Proppe, A. H.; Arquer, F. P. G. d.; Rossouw, D.; Voznyy, O.; Lan, X.; Liu, M.; Walters, G.; Quintero-Bermudez, R.; Sun, B.; Hoogland, S.; Botton, G. A.; Kelley, S. O.; Sargent, E. H. Mixed-Quantum-Dot Solar Cells. *Nat. Commun.* **2017**, *8*, 1325.

(26) Kubicki, D. J.; Prochowicz, D.; Hofstetter, A.; Zakeeruddin, S. M.; Grätzel, M.; Emsley, L. Phase Segregation in Cs-, Rb- and K-Doped Mixed-Cation $(MA)_x(FA)_{1-x}PbI_3$ Hybrid Perovskites from Solid-State NMR. *J. Am. Chem. Soc.* **2017**, *139*, 14173−14180.

(27) Han, Z.; Qiu, F.; Eisenberg, R.; Holland, P. L.; Krauss, T. D. Robust Photogeneration of H_2 in Water Using Semiconductor Nanocrystals and a Nickel Catalyst. *Science* **2012**, *338*, 1321−1324.

(28) Jensen, S. C.; Bettis Homan, S.; Weiss, E. A. Photocatalytic Conversion of Nitrobenzene to Aniline through Sequential Proton-Coupled One-Electron Transfers from a Cadmium Sulfide Quantum Dot. *J. Am. Chem. Soc.* **2016**, *138*, 1591−1600.

(29) Caputo, J. A.; Frenette, L. C.; Zhao, N.; Sowers, K. L.; Krauss, T. D.; Weix, D. J. General and Efficient C−C Bond Forming Photoredox Catalysis with Semiconductor Quantum Dots. *J. Am. Chem. Soc.* **2017**, *139*, 4250−4253.

(30) Kamat, P. V. Semiconductor Surface Chemistry as Holy Grail in Photocatalysis and Photovoltaics. *Acc. Chem. Res.* **2017**, *50*, 527−531.

(31) Bruchez, M.; Moronne, M.; Gin, P.; Weiss, S.; Alivisatos, A. P. Semiconductor Nanocrystals as Fluorescent Biological Labels. *Science* **1998**, *281*, 2013−2016.

(32) Kairdolf, B. A.; Smith, A. M.; Stokes, T. H.; Wang, M. D.; Young, A. N.; Nie, S. Semiconductor Quantum Dots for Bioimaging and Biodiagnostic Applications. *Annu. Rev. Anal. Chem.* **2013**, *6*, 143−162.

(33) Li, J.; Zhu, J.-J. Quantum Dots for Fluorescent Biosensing and Bio-Imaging Applications. *Analyst* **2013**, *138*, 2506−2515.

(34) Chen, O.; Zhao, J.; Chauhan, V. P.; Cui, J.; Wong, C.; Harris, D. K.; Wei, H.; Han, H.-S.; Fukumura, D.; Jain, R. K.; Bawendi, M. G. Compact High-Quality CdSe−CdS Core−Shell Nanocrystals with Narrow Emission Linewidths and Suppressed Blinking. *Nat. Mater.* **2013**, *12*, 445−451.

(35) Hens, Z.; Moreels, I.; Martins, J. C. In Situ ^{1}H NMR Study on the Trioctylphosphine Oxide Capping of Colloidal InP Nanocrystals. *ChemPhysChem* **2005**, *6*, 2578−2584.

(36) Owen, J. S.; Park, J.; Trudeau, P.-E.; Alivisatos, A. P. Reaction Chemistry and Ligand Exchange at Cadmium−Selenide Nanocrystal Surfaces. *J. Am. Chem. Soc.* **2008**, *130*, 12279−12281.

(37) Hassinen, A.; Moreels, I.; de Mello Donegá, C.; Martins, J. C.; Hens, Z. Nuclear Magnetic Resonance Spectroscopy Demonstrating Dynamic Stabilization of CdSe Quantum Dots by Alkylamines. *J. Phys. Chem. Lett.* **2010**, *1*, 2577−2581.

(38) Gomes, R.; Hassinen, A.; Szczygiel, A.; Zhao, Q.; Vantomme, A.; Martins, J. C.; Hens, Z. Binding of Phosphonic Acids to CdSe Quantum Dots: A Solution NMR Study. *J. Phys. Chem. Lett.* **2011**, *2*, 145−152.

(39) Anderson, N. C.; Hendricks, M. P.; Choi, J. J.; Owen, J. S. Ligand Exchange and the Stoichiometry of Metal Chalcogenide Nanocrystals: Spectroscopic Observation of Facile Metal-Carboxylate Displacement and Binding. *J. Am. Chem. Soc.* **2013**, *135*, 18536−18548.

DOI: 10.1021/acscentsci.8b00196
ACS Cent. Sci. 2018, 4, 1113−1125

(40) Hens, Z.; Martins, J. C. A Solution NMR Toolbox for Characterizing the Surface Chemistry of Colloidal Nanocrystals. *Chem. Mater.* **2013**, *25*, 1211−1221.
(41) Anderson, N. C.; Owen, J. S. Soluble, Chloride-Terminated CdSe Nanocrystals: Ligand Exchange Monitored by ^{1}H and ^{31}P NMR Spectroscopy. *Chem. Mater.* **2013**, *25*, 69−76.
(42) Chen, P. E.; Anderson, N. C.; Norman, Z. M.; Owen, J. S. Tight Binding of Carboxylate, Phosphonate, and Carbamate Anions to Stoichiometric CdSe Nanocrystals. *J. Am. Chem. Soc.* **2017**, *139*, 3227−3236.
(43) Thayer, A. M.; Steigerwald, M. L.; Duncan, T. M.; Douglass, D. C. NMR Study of Semiconductor Molecular Clusters. *Phys. Rev. Lett.* **1988**, *60*, 2673−2676.
(44) Becerra, L. R.; Murray, C. B.; Griffin, R. G.; Bawendi, M. G. Investigation of the Surface Morphology of Capped CdSe Nanocrystallites by ^{31}P Nuclear Magnetic Resonance. *J. Chem. Phys.* **1994**, *100*, 3297−3300.
(45) Tomaselli, M.; Yarger, J. L.; Bruchez, M.; Havlin, R. H.; deGraw, D.; Pines, A.; Alivisatos, A. P. NMR Study of InP Quantum Dots: Surface Structure and Size Effects. *J. Chem. Phys.* **1999**, *110*, 8861−8864.
(46) Ratcliffe, C. I.; Yu, K.; Ripmeester, J. A.; Badruz Zaman, M.; Badarau, C.; Singh, S. Solid State NMR Studies of Photoluminescent Cadmium Chalcogenide Nanoparticles. *Phys. Chem. Chem. Phys.* **2006**, *8*, 3510−3519.
(47) Moreels, I.; Martins, J. C.; Hens, Z. Solution NMR Techniques for Investigating Colloidal Nanocrystal Ligands: A Case Study on Trioctylphosphine Oxide at InP Quantum Dots. *Sens. Actuators, B* **2007**, *126*, 283−288.
(48) Lovingood, D. D.; Achey, R.; Paravastu, A. K.; Strouse, G. F. Size- and Site-Dependent Reconstruction in CdSe QDs Evidenced by $^{77}Se\{^{1}H\}$ CP-MAS NMR Spectroscopy. *J. Am. Chem. Soc.* **2010**, *132*, 3344−3354.
(49) Protesescu, L.; Rossini, A. J.; Kriegner, D.; Valla, M.; de Kergommeaux, A.; Walter, M.; Kravchyk, K. V.; Nachtegaal, M.; Stangl, J.; Malaman, B.; Reiss, P.; Lesage, A.; Emsley, L.; Copéret, C.; Kovalenko, M. V. Unraveling the Core−Shell Structure of Ligand-Capped Sn/SnO_x Nanoparticles by Surface-Enhanced Nuclear Magnetic Resonance, Mössbauer, and X-ray Absorption Spectroscopies. *ACS Nano* **2014**, *8*, 2639−2648.
(50) Piveteau, L.; Ong, T.-C.; Rossini, A. J.; Emsley, L.; Copéret, C.; Kovalenko, M. V. Structure of Colloidal Quantum Dots from Dynamic Nuclear Polarization Surface Enhanced NMR Spectroscopy. *J. Am. Chem. Soc.* **2015**, *137*, 13964−13971.
(51) Protesescu, L.; Nachtegaal, M.; Voznyy, O.; Borovinskaya, O.; Rossini, A. J.; Emsley, L.; Copéret, C.; Günther, D.; Sargent, E. H.; Kovalenko, M. V. Atomistic Description of Thiostannate-Capped CdSe Nanocrystals: Retention of Four-Coordinate SnS_4 Motif and Preservation of Cd-Rich Stoichiometry. *J. Am. Chem. Soc.* **2015**, *137*, 1862−1874.
(52) Fiurasek, P.; Reven, L. Phosphonic and Sulfonic Acid-Functionalized Gold Nanoparticles: A Solid-State NMR Study. *Langmuir* **2007**, *23*, 2857−2866.
(53) Smith, A. M.; Millstone, J. E. In *Biomedical Nanotechnology: Methods and Protocols*; Petrosko, S. H., Day, E. S., Eds.; Springer: New York, NY, 2017; pp 17−29.
(54) Sachleben, J. R.; Wooten, E. W.; Emsley, L.; Pines, A.; Colvin, V. L.; Alivisatos, A. P. NMR Studies of the Surface Structure and Dynamics of Semiconductor Nanocrystals. *Chem. Phys. Lett.* **1992**, *198*, 431−436.
(55) Cadars, S.; Smith, B. J.; Epping, J. D.; Acharya, S.; Belman, N.; Golan, Y.; Chmelka, B. F. Atomic Positional Versus Electronic Order in Semiconducting ZnSe Nanoparticles. *Phys. Rev. Lett.* **2009**, *103*, 1368021−1368024.
(56) Berrettini, M. G.; Braun, G.; Hu, J. G.; Strouse, G. F. NMR Analysis of Surfaces and Interfaces in 2-nm CdSe. *J. Am. Chem. Soc.* **2004**, *126*, 7063−7070.
(57) Marbella, L. E.; Gan, X. Y.; Kaseman, D. C.; Millstone, J. E. Correlating Carrier Density and Emergent Plasmonic Features in $Cu_{2-x}Se$ Nanoparticles. *Nano Lett.* **2017**, *17*, 2414−2419.
(58) Spataro, G.; Champouret, Y.; Florian, P.; Coppel, Y.; Kahn, M. L. Multinuclear Solid-State NMR Study: a Powerful Tool for Understanding the Structure of ZnO Hybrid Nanoparticles. *Phys. Chem. Chem. Phys.* **2018**, *20*, 12413−12421.
(59) Maly, T.; Debelouchina, G. T.; Bajaj, V. S.; Hu, K.-N.; Joo, C.-G.; Mak-Jurkauskas, M. L.; Sirigiri, J. R.; van der Wel, P. C. A.; Herzfeld, J.; Temkin, R. J.; Griffin, R. G. Dynamic Nuclear Polarization at High Magnetic Fields. *J. Chem. Phys.* **2008**, *128*, 052211.
(60) Ni, Q. Z.; Daviso, E.; Can, T. V.; Markhasin, E.; Jawla, S. K.; Swager, T. M.; Temkin, R. J.; Herzfeld, J.; Griffin, R. G. High Frequency Dynamic Nuclear Polarization. *Acc. Chem. Res.* **2013**, *46*, 1933−1941.
(61) Becerra, L. R.; Gerfen, G. J.; Bellew, B. F.; Bryant, J. A.; Hall, D. A.; Inati, S. J.; Weber, R. T.; Un, S.; Prisner, T. F.; McDermott, A. E.; Fishbein, K. W.; Kreischer, K. E.; Temkin, R. J.; Singel, D. J.; Griffin, R. G. A Spectrometer for Dynamic Nuclear Polarization and Electron Paramagnetic Resonance at High Frequencies. *J. Magn. Reson., Ser. A* **1995**, *117*, 28−40.
(62) Lesage, A.; Lelli, M.; Gajan, D.; Caporini, M. A.; Vitzthum, V.; Miéville, P.; Alauzun, J.; Roussey, A.; Thieuleux, C.; Mehdi, A.; Bodenhausen, G.; Copéret, C.; Emsley, L. Surface Enhanced NMR Spectroscopy by Dynamic Nuclear Polarization. *J. Am. Chem. Soc.* **2010**, *132*, 15459−15461.
(63) Rossini, A. J.; Zagdoun, A.; Lelli, M.; Lesage, A.; Copéret, C.; Emsley, L. Dynamic Nuclear Polarization Surface Enhanced NMR Spectroscopy. *Acc. Chem. Res.* **2013**, *46*, 1942−1951.
(64) Kobayashi, T.; Perras, F. A.; Slowing, I. I.; Sadow, A. D.; Pruski, M. Dynamic Nuclear Polarization Solid-State NMR in Heterogeneous Catalysis Research. *ACS Catal.* **2015**, *5*, 7055−7062.
(65) Copéret, C.; Liao, W.-C.; Gordon, C. P.; Ong, T.-C. Active Sites in Supported Single-Site Catalysts: An NMR Perspective. *J. Am. Chem. Soc.* **2017**, *139*, 10588−10596.
(66) Viger-Gravel, J.; Berruyer, P.; Gajan, D.; Basset, J.-M.; Lesage, A.; Tordo, P.; Ouari, O.; Emsley, L. Frozen Acrylamide Gels as Dynamic Nuclear Polarization Matrices. *Angew. Chem., Int. Ed.* **2017**, *56*, 8726−8730.
(67) Hall, D. A.; Maus, D. C.; Gerfen, G. J.; Inati, S. J.; Becerra, L. R.; Dahlquist, F. W.; Griffin, R. G. Polarization-Enhanced NMR Spectroscopy of Biomolecules in Frozen Solution. *Science* **1997**, *276*, 930−932.
(68) Kubicki, D. J.; Casano, G.; Schwarzwalder, M.; Abel, S.; Sauvee, C.; Ganesan, K.; Yulikov, M.; Rossini, A. J.; Jeschke, G.; Copéret, C.; Lesage, A.; Tordo, P.; Ouari, O.; Emsley, L. Rational Design of Dinitroxide Biradicals for Efficient Cross-Effect Dynamic Nuclear Polarization. *Chem. Sci.* **2016**, *7*, 550−558.
(69) Silverio, D. L.; van Kalkeren, H. A.; Ong, T.-C.; Baudin, M.; Yulikov, M.; Veyre, L.; Berruyer, P.; Chaudhari, S.; Gajan, D.; Baudouin, D.; Cavaillès, M.; Vuichoud, B.; Bornet, A.; Jeschke, G.; Bodenhausen, G.; Lesage, A.; Emsley, L.; Jannin, S.; Thieuleux, C.; Copéret, C. Tailored Polarizing Hybrid Solids with Nitroxide Radicals Localized in Mesostructured Silica Walls. *Helv. Chim. Acta* **2017**, *100*, e1700101.
(70) Dixon, W. T. Spinning-Sideband-Free and Spinning-Sideband-Only NMR Spectra in Spinning Samples. *J. Chem. Phys.* **1982**, *77*, 1800−1809.
(71) Antzutkin, O. N.; Shekar, S. C.; Levitt, M. H. Two-Dimensional Sideband Separation in Magic-Angle-Spinning NMR. *J. Magn. Reson., Ser. A* **1995**, *115*, 7−19.
(72) Hu, J. Z.; Alderman, D. W.; Ye, C. H.; Pugmire, R. J.; Grant, D. M. An Isotropic Chemical Shift-Chemical Shift Anisotropy Magic-Angle Slow-Spinning 2D NMR Experiment. *J. Magn. Reson., Ser. A* **1993**, *105*, 82−87.
(73) Gan, Z. High-Resolution Chemical Shift and Chemical Shift Anisotropy Correlation in Solids using Slow Magic Angle Spinning. *J. Am. Chem. Soc.* **1992**, *114*, 8307−8309.
(74) Gann, S. L.; Baltisberger, J. H.; Pines, A. Dynamic-Angle Spinning without Sidebands. *Chem. Phys. Lett.* **1993**, *210*, 405−410.
(75) Hung, I.; Edwards, T.; Sen, S.; Gan, Z. MATPASS/CPMG: A Sensitivity Enhanced Magic-Angle Spinning Sideband Separation Experiment for Disordered Solids. *J. Magn. Reson.* **2012**, *221*, 103−109.

DOI: 10.1021/acscentsci.8b00196
ACS Cent. Sci. 2018, 4, 1113−1125

(76) Walder, B. J.; Dey, K. K.; Kaseman, D. C.; Baltisberger, J. H.; Grandinetti, P. J. Sideband Separation Experiments in NMR with Phase Incremented Echo Train Acquisition. *J. Chem. Phys.* **2013**, *138*, 174203.
(77) Matsunaga, T.; Takegoshi, K. Magic-Angle Turning with Double Acquisition. *J. Magn. Reson.* **2017**, *274*, 1−6.
(78) Clément, R. J.; Pell, A. J.; Middlemiss, D. S.; Strobridge, F. C.; Miller, J. K.; Whittingham, M. S.; Emsley, L.; Grey, C. P.; Pintacuda, G. Spin-Transfer Pathways in Paramagnetic Lithium Transition-Metal Phosphates from Combined Broadband Isotropic Solid-State MAS NMR Spectroscopy and DFT Calculations. *J. Am. Chem. Soc.* **2012**, *134*, 17178−17185.
(79) Perras, F. A.; Venkatesh, A.; Hanrahan, M. P.; Goh, T. W.; Huang, W.; Rossini, A. J.; Pruski, M. Indirect Detection of Infinite-Speed MAS Solid-State NMR Spectra. *J. Magn. Reson.* **2017**, *276*, 95−102.
(80) Baltisberger, J. H.; Walder, B. J.; Keeler, E. G.; Kaseman, D. C.; Sanders, K. J.; Grandinetti, P. J. Communication: Phase Incremented Echo Train Acquisition in NMR Spectroscopy. *J. Chem. Phys.* **2012**, *136*, 211104.
(81) Wolf, P.; Valla, M.; Rossini, A. J.; Comas-Vives, A.; Núñez-Zarur, F.; Malaman, B.; Lesage, A.; Emsley, L.; Copéret, C.; Hermans, I. NMR Signatures of the Active Sites in Sn-β Zeolite. *Angew. Chem., Int. Ed.* **2014**, *53*, 10179−10183.
(82) Alphazan, T.; Mathey, L.; Schwarzwälder, M.; Lin, T.-H.; Rossini, A. J.; Wischert, R.; Enyedi, V.; Fontaine, H.; Veillerot, M.; Lesage, A.; Emsley, L.; Veyre, L.; Martin, F.; Thieuleux, C.; Copéret, C. Monolayer Doping of Silicon through Grafting a Tailored Molecular Phosphorus Precursor onto Oxide-Passivated Silicon Surfaces. *Chem. Mater.* **2016**, *28*, 3634−3640.
(83) Ong, T.-C.; Liao, W.-C.; Mougel, V.; Gajan, D.; Lesage, A.; Emsley, L.; Copéret, C. Atomistic Description of Reaction Intermediates for Supported Metathesis Catalysts Enabled by DNP SENS. *Angew. Chem.* **2016**, *128*, 4821−4825.
(84) Chen, O.; Chen, X.; Yang, Y.; Lynch, J.; Wu, H.; Zhuang, J.; Cao, Y. C. Synthesis of Metal−Selenide Nanocrystals Using Selenium Dioxide as the Selenium Precursor. *Angew. Chem., Int. Ed.* **2008**, *47*, 8638−8641.
(85) Li, J. J.; Wang, Y. A.; Guo, W.; Keay, J. C.; Mishima, T. D.; Johnson, M. B.; Peng, X. Large-Scale Synthesis of Nearly Monodisperse CdSe/CdS Core/Shell Nanocrystals Using Air-Stable Reagents via Successive Ion Layer Adsorption and Reaction. *J. Am. Chem. Soc.* **2003**, *125*, 12567−12575.
(86) Cossairt, B. M.; Owen, J. S. CdSe Clusters: At the Interface of Small Molecules and Quantum Dots. *Chem. Mater.* **2011**, *23*, 3114−3119.
(87) Ithurria, S.; Tessier, M. D.; Mahler, B.; Lobo, R. P. S. M.; Dubertret, B.; Efros, A. L. Colloidal Nanoplatelets with Two-Dimensional Electronic Structure. *Nat. Mater.* **2011**, *10*, 936−941.
(88) Ithurria, S.; Talapin, D. V. Colloidal Atomic Layer Deposition (c-ALD) using Self-Limiting Reactions at Nanocrystal Surface Coupled to Phase Transfer between Polar and Nonpolar Media. *J. Am. Chem. Soc.* **2012**, *134*, 18585−18590.
(89) Tessier, M. D.; Spinicelli, P.; Dupont, D.; Patriarche, G.; Ithurria, S.; Dubertret, B. Efficient Exciton Concentrators Built from Colloidal Core/Crown CdSe/CdS Semiconductor Nanoplatelets. *Nano Lett.* **2014**, *14*, 207−213.
(90) Pines, A.; Gibby, M. G.; Waugh, J. S. Proton-Enhanced NMR of Dilute Spins in Solids. *J. Chem. Phys.* **1973**, *59*, 569−590.
(91) Wilson, P. J. In *Annual Reports on NMR Spectroscopy*; Academic Press: Cambridge, MA, 2003; Vol. *49*, pp 117−168.
(92) Gauss, J.; Stanton, J. F. In *Calculation of NMR and EPR Parameters*; Wiley-VCH Verlag GmbH & Co. KGaA: Weinheim, Germany, 2004; pp 123−139.
(93) Matsuki, Y.; Maly, T.; Ouari, O.; Karoui, H.; Le Moigne, F.; Rizzato, E.; Lyubenova, S.; Herzfeld, J.; Prisner, T.; Tordo, P.; Griffin, R. G. Dynamic Nuclear Polarization with a Rigid Biradical. *Angew. Chem., Int. Ed.* **2009**, *48*, 4996−5000.
(94) Zagdoun, A.; Rossini, A. J.; Gajan, D.; Bourdolle, A.; Ouari, O.; Rosay, M.; Maas, W. E.; Tordo, P.; Lelli, M.; Emsley, L.; Lesage, A.; Copéret, C. Non-Aqueous Solvents for DNP Surface Enhanced NMR Spectroscopy. *Chem. Commun.* **2012**, *48*, 654−656.
(95) Schaefer, J.; Stejskal, E. O. Carbon-13 Nuclear Magnetic Resonance of Polymers psinning at the Magic Angle. *J. Am. Chem. Soc.* **1976**, *98*, 1031−1032.
(96) Ithurria, S.; Bousquet, G.; Dubertret, B. Continuous Transition from 3D to 1D Confinement Observed during the Formation of CdSe Nanoplatelets. *J. Am. Chem. Soc.* **2011**, *133*, 3070−3077.
(97) She, C.; Fedin, I.; Dolzhnikov, D. S.; Demortière, A.; Schaller, R. D.; Pelton, M.; Talapin, D. V. Low-Threshold Stimulated Emission Using Colloidal Quantum Wells. *Nano Lett.* **2014**, *14*, 2772−2777.
(98) Liu, L.; Zhuang, Z.; Xie, T.; Wang, Y.-G.; Li, J.; Peng, Q.; Li, Y. Shape Control of CdSe Nanocrystals with Zinc Blende Structure. *J. Am. Chem. Soc.* **2009**, *131*, 16423−16429.
(99) Prudnikau, A.; Chuvilin, A.; Artemyev, M. CdSe−CdS Nanoheteroplatelets with Efficient Photoexcitation of Central CdSe Region through Epitaxially Grown CdS Wings. *J. Am. Chem. Soc.* **2013**, *135*, 14476−14479.
(100) Kelestemur, Y.; Guzelturk, B.; Erdem, O.; Olutas, M.; Gungor, K.; Demir, H. V. Colloidal Nanoplatelets: Platelet-in-Box Colloidal Quantum Wells: CdSe/CdS@CdS Core/Crown@Shell Heteronanoplatelets. *Adv. Funct. Mater.* **2016**, *26*, 3554−3554.
(101) Tessier, M. D.; Mahler, B.; Nadal, B.; Heuclin, H.; Pedetti, S.; Dubertret, B. Spectroscopy of Colloidal Semiconductor Core/Shell Nanoplatelets with High Quantum Yield. *Nano Lett.* **2013**, *13*, 3321−3328.
(102) Mahler, B.; Nadal, B.; Bouet, C.; Patriarche, G.; Dubertret, B. Core/Shell Colloidal Semiconductor Nanoplatelets. *J. Am. Chem. Soc.* **2012**, *134*, 18591−18598.
(103) Rempel, J. Y.; Trout, B. L.; Bawendi, M. G.; Jensen, K. F. Density Functional Theory Study of Ligand Binding on CdSe (0001), (000$\bar{1}$), and (11$\bar{2}$0) Single Crystal Relaxed and Reconstructed Surfaces: Implications for Nanocrystalline Growth. *J. Phys. Chem. B* **2006**, *110*, 18007−18016.
(104) Puzder, A.; Williamson, A. J.; Zaitseva, N.; Galli, G.; Manna, L.; Alivisatos, A. P. The Effect of Organic Ligand Binding on the Growth of CdSe Nanoparticles Probed by Ab Initio Calculations. *Nano Lett.* **2004**, *4*, 2361−2365.
(105) Shiang, J. J.; Kadavanich, A. V.; Grubbs, R. K.; Alivisatos, A. P. Symmetry of Annealed Wurtzite CdSe Nanocrystals: Assignment to the C3v Point Group. *J. Phys. Chem.* **1995**, *99*, 17417−17422.
(106) Beecher, A. N.; Yang, X.; Palmer, J. H.; LaGrassa, A. L.; Juhas, P.; Billinge, S. J. L.; Owen, J. S. Atomic Structures and Gram Scale Synthesis of Three Tetrahedral Quantum Dots. *J. Am. Chem. Soc.* **2014**, *136*, 10645−10653.
(107) Czjzek, G.; Fink, J.; Götz, F.; Schmidt, H.; Coey, J. M. D.; Rebouillat, J. P.; Liénard, A. Atomic Coordination and the Distribution of Electric Field Gradients in Amorphous Solids. *Phys. Rev. B: Condens. Matter Mater. Phys.* **1981**, *23*, 2513−2530.
(108) Baltisberger, J. H.; Florian, P.; Keeler, E. G.; Phyo, P. A.; Sanders, K. J.; Grandinetti, P. J. Modifier Cation Effects on ^{29}Si Nuclear Shielding Anisotropies in Silicate Glasses. *J. Magn. Reson.* **2016**, *268*, 95−106.
(109) Zagdoun, A.; Casano, G.; Ouari, O.; Schwarzwälder, M.; Rossini, A. J.; Aussenac, F.; Yulikov, M.; Jeschke, G.; Copéret, C.; Lesage, A.; Tordo, P.; Emsley, L. Large Molecular Weight Nitroxide Biradicals Providing Efficient Dynamic Nuclear Polarization at Temperatures up to 200 K. *J. Am. Chem. Soc.* **2013**, *135*, 12790−12797.
(110) Rosay, M.; Tometich, L.; Pawsey, S.; Bader, R.; Schauwecker, R.; Blank, M.; Borchard, P. M.; Cauffman, S. R.; Felch, K. L.; Weber, R. T.; Temkin, R. J.; Griffin, R. G.; Maas, W. E. Solid-State Dynamic Nuclear Polarization at 263 GHz: Spectrometer Design and Experimental Results. *Phys. Chem. Chem. Phys.* **2010**, *12*, 5850−5860.
(111) Peersen, O. B.; Wu, X. L.; Kustanovich, I.; Smith, S. O. Variable-Amplitude Cross-Polarization MAS NMR. *J. Magn. Reson., Ser. A* **1993**, *104*, 334−339.
(112) Fung, B. M.; Khitrin, A. K.; Ermolaev, K. An Improved Broadband Decoupling Sequence for Liquid Crystals and Solids. *J. Magn. Reson.* **2000**, *142*, 97−101.

DOI: 10.1021/acscentsci.8b00196
ACS Cent. Sci. 2018, 4, 1113−1125